Pseudopaline, a staphylopine-like metallophore involved in zinc and nickel uptake in *Pseudomonas aeruginosa*

Sébastien Lhospice[1,§], Nicolas Oswaldo Gomez[1,§], Laurent Ouerdane[2,§], Catherine Brutesco[3], Ghassan Ghssein[3], Christine Hajjar[3], Ahmed Liratni[1], Shuanglong Wang[2], Pierre Richaud[4], Sophie Bleves[1], Geneviève Ball[1], Elise Borezée-Durant[5], Ryszard Lobinski[2], David Pignol[3], Pascal Arnoux[3,*] and Romé Voulhoux[1,*]

[1]CNRS et Aix-Marseille Université, Laboratoire d'Ingénierie des Systèmes Macromoléculaires (UMR7255), Institut de Microbiologie de la Méditerranée, Marseille, France.

[2]Université de Pau et des Pays de l'Adour/CNRS, Laboratoire de Chimie Analytique Bio-inorganique et Environnement, IPREM-UMR5254, Hélioparc, 2, Avenue Angot, 64053 Pau, France.

[3]CEA, CNRS and Aix-Marseille Université, Institut de Biosciences et Biotechnologies d'Aix-Marseille, UMR 7265 LBC, CEA Cadarache, Saint-Paul-lez-Durance F-13108, France.

[4]CEA, CNRS and Aix-Marseille Université, Institut de Biosciences et Biotechnologies d'Aix-Marseille, UMR 7265 LB3M, CEA Cadarache, Saint-Paul-lez Durance F-13108, France.

[5]Micalis Institute, INRA, AgroParisTech, Université Paris-Saclay, 78350 Jouy-en-Josas, France.

[§]Contributed equally to this work

[*]Correspondence E-mail: pascal.arnoux@cea.fr and voulhoux@imm.cnrs.fr

ABSTRACT

Metal uptake is vital for all living organisms. In metal scarce conditions, a common bacterial strategy consists in the biosynthesis of metallophores, their export in the extracellular medium and the recovery of a metal-metallophore complex through dedicated membrane transporters. Staphylopine is a recently described metallophore distantly related to plant nicotianamine that contributes to the broad-spectrum metal uptake capabilities of *Staphylococcus aureus*. Here, we characterize a four genes operon (*PA4837–PA4834*) in *Pseudomonas aeruginosa* involved in the biosynthesis and trafficking of a staphylopine-like metallophore named pseudopaline. Pseudopaline differs from staphylopine with regard to the stereochemistry of its histidine moiety associated to an alpha ketoglutarate moiety instead of pyruvate. *In vivo*, the pseudopaline operon is regulated by zinc through the Zur repressor. The metal-uptake property of the pseudopaline system appears different from that of staphylopine with a predominant effect on nickel uptake, and on zinc uptake in metal scarce conditions mimicking a chelating environment, thus reconciling the regulation of the *cnt* operon by zinc with its function as a zinc importer under metal scarce conditions.

SIGNIFICANCE

Zinc is an essential micronutrients for bacteria, particularly important at the host-pathogen interface where the host tends to sequester metals in a so called nutritional immunity framework, and the pathogenic bacterium increases its metal uptake efforts in order to keep up with its metal requirements. Here we reveal a novel metallophore, named pseudopaline, which is synthesized and exported by *Pseudomonas aeruginosa* and serves for the uptake of nickel in metal poor media, and for the uptake of zinc in metal scarce conditions that mimic the chelating environment that presumably prevails within a host.

INTRODUCTION

Divalent metals (Mn, Fe, Co, Ni, Cu and Zn) are essential micronutrients for all life forms, and acquisition of these metals is therefore vital, particularly for bacterial pathogens in the context of host-pathogen interactions. Indeed, there is a competition between the host, which tends to sequester metals in a so called nutritional immunity framework, and the pathogenic bacterium, which increases its metal uptake efforts in order to keep up with its metal requirements (1, 2). Most pathogenic bacteria produce metallophores for metal uptake, with siderophores being the most well-characterized metallophore family (3). Siderophores are synthesized within the cell through non ribosomal peptide synthases (NRPS) or through a NRPS independent system (NIS) and then are exported in the extracellular medium where they scavenge iron. Extracellular iron siderophore complexes can be recognized and actively transported into the periplasm by TonB dependent transporters (TBDT) in Gram-negative bacteria, and usually ABC transporters in both Gram-negative and Gram-positive bacteria are used for the crossing of the cytoplasmic membrane. There are many variations on this common theme and, for example, some bacteria do not produce a specific type of siderophore although they are able to use it for iron import (4). The siderophore pathway could also prevent toxic accumulation of metals, which was particularly studied in the case of *Pseudomonas aeruginosa* (5, 6). *P. aeruginosa* synthesizes two types of siderophores with high iron affinity, pyochelin and pyoverdine, the latter being a demonstrated virulence factor (7).

Metallophores specific for the uptake of metals other than iron have also been described, such as the chalcophore methanobactin involved in copper uptake in methane-oxidizing bacteria (8, 9). Manganesophore have not been described as such, although TseM, a protein effector secreted through a Type VI secretion system, was shown to play an important role in TBDT-dependent manganese uptake in *Burkholderia thailandensis* (10). There is also indirect evidence for the existence of a nickelophore in *Escherichia coli*, although it has still to be identified (11). Free histidine could also be used as a nickelophore *in vivo* for nickel uptake in various bacteria (12, 13). Yersiniabactin, initially described as a siderophore, also exhibits zincophore properties in *Yersinia pestis* (14, 15). Coelibactin, described in *Streptomyces coelicolor*, may also represent a zincophore as it is synthesized by a NRPS under the control of Zur, a zinc responsive repressor (16).

Staphylopine is a nicotianamine-like molecule that was recently described as a metallophore with remarkable broad-spectrum specificity (17). In *Staphylococcus aureus*, staphylopine is synthesized through the action of three soluble enzymes (SaCntKLM). SaCntK transforms L-

histidine in D-histidine, SaCntL transfers an aminobutyrate moiety from S-adenosylmethionine (SAM) onto D-histidine, and SaCntM reductively condensates the product of SaCntL (called xNA) with pyruvate. The staphylopine biosynthesis and trafficking pathway is responsible for zinc, copper, nickel, cobalt and iron uptake, depending on the growth conditions, and this system contributes to the virulence and fitness of *S. aureus* (17–19). The *S. aureus cnt* operon is partly conserved in *P. aeruginosa*, where homologues of the *cntL* and *cntM* genes are found, albeit with 20-30% sequence identity at the protein level. Upstream of *cntL*, a gene codes a predicted outer membrane protein belonging to the TBDT family, and downstream of *cntM*, a gene codes for a predicted inner membrane protein belonging to the EamA or DMT family (drug/metabolite transporter; Figure S1). Transcriptomic approaches revealed that this gene cluster was highly expressed in a burn wound model (20). This last gene was also identified as part of a novel siderophore pathway that appeared vital for the growth of *P. aeruginosa* in airway mucus secretion (AMS) (21). Finally, through a transcriptomic study of a Zur deficient strain, these four genes were found in the top five regulated units, although most of them were annotated as hypothetical (22).

Here, we show that the four above-mentioned genes (here named *cntO*, *cntL*, *cntM* and *cntI;* see supplementary table S1 for correspondence with locus tag in PAO1, PA7 and PA14 strains of *P. aeruginosa*) are part of an operon that is regulated by zinc level through the Zur repressor. Using biochemistry and metabolomics approaches, we prove that the two biosynthetic enzymes (PaCntL and PaCntM) synthesize a novel metallophore, which we named pseudopaline, and which differs from staphylopine by the presence of a D-histidine moiety instead of L-histidine, and an α-ketoglutarate moiety instead of a pyruvate. A *cntL* mutant strain is shown to be unable to synthesize pseudopaline and is impaired in its ability to import nickel in a minimal media, supplemented or not with nickel. Under more stringent conditions where a chelator such as EDTA is added to a minimal succinate (MS) medium, a condition that presumably mimics the chelating environment prevailing within a host or in AMS, we show evidence that the *cntL* mutant strain is unable to import zinc, therefore reconciling the regulation of this operon by zinc with its function as a zinc importer functioning in metal scarce conditions.

Results and discussion

The *cnt* operon of *P. aeruginosa* is regulated by zinc level through the zinc-responsive regulator Zur

In silico analysis of the *cnt* gene cluster of *P. aeruginosa* PA14 strain indicated two overlapping open reading frames between *cntL* and *cntM* and between *cntM* and *cntI*, classically observed in operonic structures (Figure S1). Further screening of the upstream *cnt* sequence for promoter regions using Bprom software (23), revealed a σ70 promoter in the 200 base-pairs upstream from the annotated *cntO* ATG codon (Figure S1). Interestingly, a putative Zur binding box "GTTATagtATAtC" can be identified overlapping the -10 box of the predicted σ70 promoter, (22, 24). This *in silico* analysis supports an operonic organization of the four *cnt* genes and strongly suggests a transcriptional activation of this operon under zinc depletion through the Zur repressor (25, 26). In order to test this hypothesis, we performed RT-PCR experiments using as templates RNA and cDNA generated from a WT PA14 strain grown in minimal succinate (MS) medium known to contains low levels of metals, including zinc (5). The successful amplification of the four *cnt* gene transcripts (Figure S1) indeed indicated their induction when cells were grown in a MS medium. The specific amplification of the three *cnt* intergenic regions confirmed that the four *cnt* genes are co-transcribed in one single transcript and therefore constitute an operon.

To validate at the protein level the transcriptional regulation of the *cnt* genes, we followed by immunoblotting the PaCntL production under various growth conditions. In this respect, we constructed a *cntL* mutant strain producing a chromosomally encoded V5-tagged PaCntL (Δ*cntL::cntL*$_{V5}$). In this strain, the recombinant *cntL*$_{V5}$ gene was placed under the predicted *cnt* promoter region and inserted at the *att* site of the *P. aeruginosa* genome. In agreement with our transcriptional data, immunoblotting experiments indicated that, the recombinant PaCntL$_{V5}$ is only produced in MS medium and not in a rich medium such as the LB medium (Figure 1A). Presumably, this is due to the low metal content of the MS medium as compared to the LB medium. We then tested whether the *cntL* transcription was subject to metal repression by checking PaCntL$_{V5}$ production in MS medium supplemented with various concentrations of the most representative metals. Dot-blot experiments showed a specific loss of PaCntL$_{V5}$ production in MS medium supplemented with as low as 0.1 µM of $ZnSO_4$. An addition of iron, nickel or cobalt at concentrations equivalent or above the one found in LB rich medium (5) has no negative effect on PaCntL$_{V5}$ production (Figure 1B). The hypothesis of a Zur repressor regulating the *cnt* operon was then tested through the construction of a PA14Δ*cntL::cntL*$_{V5}$ *zur*$^{-}$ strain. PaCntL$_{V5}$ was still produced in the *zur* mutant strain grown in

LB or MS media supplemented with 1 μM of $ZnSO_4$, conditions in which Zur normally exerts its repressor activity (Figure 1C). Taken together, these data therefore demonstrate that the *cnt* operon of *P. aeruginosa* is negatively regulated by zinc, most probably through the binding of a Zn-Zur repressor complex onto the predicted Zur binding motif identified in the σ70 promoter, thus preventing the recruitment of RNA-polymerase.

In vivo detection and characterization of a PaCntL-dependent metallophore in the extracellular medium of *P. aeruginosa*

We constructed a PA14 mutant strain lacking PaCntL (Δ*cntL*) and compared the composition of the intra- and extra-cellular contents of wild type and Δ*cntL* strains grown under the previously defined *cnt* inducible conditions. Extracellular samples were analysed by hydrophilic interaction liquid chromatography (HILIC) with detection by inductively coupled plasma mass spectrometry (ICP-MS) and electrospray ionization mass spectrometry (ESI-MS). HILIC/ICP-MS data revealed the presence of a molecule complexed with nickel and zinc in the supernatant of the WT strain, which was absent in the *cntL* mutant strain (Figure 2). ESI-MS investigation of the metabolites eluting at this same elution volume showed unambiguously the presence of typical nickel and zinc isotopic patterns indicating the presence of a free metallophore with a molecular mass of 386 Da (Figure 2). Using the accurate mass and a molecular formula finder software we proposed the $C_{15}N_4O_8H_{20}$ empiric formula for the ligand in complex with nickel or zinc (Figure 2, inset for the nickel chelate). This ligand corresponds to a new metallophore produced by *P. aeruginosa* in a *cntL*-dependent manner. Comparison of its elemental composition with that of staphylopine (328 Da) revealed the presence of two additional carbons and two oxygen atoms, suggesting the use of an α-ketoglutarate (αKG) moiety instead of pyruvate as found in staphylopine. The fragmentation of this metallophore in gas-phase confirmed this hypothesis (Figure S2). We propose to name this new metallophore pseudopaline, to recall its origin from *P. aeruginosa* and its belonging to the nopaline family of opine (27).

In vitro reconstitution of the pseudopaline biosynthetic pathway catalysed by PaCntL and PaCntM

We have recently shown that the PaCntL/M orthologs in *S. aureus* (SaCntL/M) are sequentially involved in the biosynthesis of the staphylopine metallophore, using a D-histidine that is produced by the histidine racemase enzyme SaCntK (17). One of the main difference between the *cnt* operons of *P. aeruginosa* and *S. aureus* is however the absence of

a *cntK* gene upstream of the *cntL-M* genes in *P. aeruginosa*. This observation led to the possibility of using directly L-histidine instead of D-histidine. In order to investigate the properties of CntL and CntM of *P. aeruginosa*, the corresponding genes were cloned, heterologously expressed in *E. coli* and their products purified for further biochemical analysis. Gel filtration experiments showed that PaCntL could form a complex with PaCntM (Figure S3), although this interaction was not observed between SaCntL and SaCntM. With regard to PaCntL, we used thin layer chromatography (TLC) separation to follow the carboxyl moiety of a carboxyl-[^{14}C]-labelled S-adenosine methionine (SAM) substrate, co-incubated with either L- or D-histidine (Figure 3A). Only the incubation with L-histidine led to a novel band corresponding to a reaction intermediate that we propose to name yNA. We demonstrated subsequently that PaCntM preferentially bound to NADH and not to NADPH (Figure 3B), contrary to SaCntM that showed a preference for NADPH. We then used TLC to visualize the PaCntLM reaction products under various *in vitro* conditions using all the putative substrates (Figure 3C). Unexpectedly, the co-incubation of both enzymes with their most probable substrates (L-histidine, NADH and αKG) did not lead to the formation of an additional radiolabelled product as for the case of staphylopine biosynthesis (17) (Figure 3C). One possibility was therefore that the product of PaCntM was migrating at the same position as the yNA in the conditions used during the TLC separation. We therefore decided to study the same co-incubations by HILIC/ESI-MS, following the mass expected for the yNA intermediate and the pseudopaline found in the extracellular fraction of *P. aeruginosa* grown in MS medium. These experiments confirmed that the incubation of PaCntL with SAM and L-histidine led to the formation of the yNA reaction intermediate (Figure 3D, top), and most of all, revealed the production of pseudopaline when co-incubating PaCntL, PaCntM and their proposed substrates (SAM, L-histidine, NADH and αKG; Figure 3D, bottom). Co-incubations using alternative substrates of PaCntM (pyruvate or NADPH) only led to the production of yNA. Interestingly, pseudopaline and yNA eluted at the same volume in these HILIC-ESI/MS experiments, showing that their physical properties are very similar, as suggested by our previous TLC experiments.

Pseudopaline is therefore biosynthesized in two steps: first, a nucleophylic attack of one α-aminobutyric acid moiety from SAM onto L-histidine catalysed by PaCntL to produce the reaction intermediate yNA, and second, a NADH reductive condensation of the yNA intermediate with a molecule of αKG catalysed by PaCntM to produce pseudopaline (Figure 3E). Pseudopaline differs from staphylopine by the stereochemistry of the histidine moiety (L- and D- respectively) and by the presence of an αKG moiety instead of pyruvate in

staphylopine. The biosynthesis of a specific metallophore by different bacteria recalls the chemical evolution of a large diversity of siderophore in a chemical rivalry to get access to one's own pool of metal (28). Indeed, once in the extracellular medium, secreted metallophores are a common good, and a privileged access presumably gives a selective advantage.

Pseudopaline is involved in nickel and zinc uptake, depending on the chelating properties of the media

In order to address the involvement of pseudopaline in metal uptake *in vivo*, we compared the intracellular concentration of various metals in PA14 WT, *ΔcntL* and *ΔcntL::cntL* strains. Cells were grown in pseudopaline-synthesis conditions determined above (MS medium) and the intracellular metal concentration was measured by ICP-MS. Under these growth conditions we observed a significant 90% reduction of intracellular nickel concentration in the *ΔcntL* mutant strain (Figure 4A), which was mostly recovered in the complemented strain. The levels of all the other metals were not changed in the *ΔcntL* mutant strain compared to the WT strain (data not shown). A similar 90% reduction in intracellular nickel concentration was also observed when the culture was supplemented with 1µM $NiCl_2$ (Figure S4), thus confirming that nickel uptake was predominantly performed by pseudopaline in these metal-poor media. We were intrigued by the apparent contradiction between the clear *cnt* operon regulation by zinc, and the absence of any effect on zinc uptake. A possible explanation is that the effect of *cnt* could be masked by the effect of a zinc ion importer such as the ZnuABC zinc transport system described in *P. aeruginosa* (22). In an attempt to discriminate between both transport systems, we sequestered free metal ions by supplementing the growth medium with increasing concentrations of EDTA, a chelating agent for divalent metals. Interestingly, although we did not observe any effect using 10 µM EDTA, the supplementation with 100µM EDTA ultimately revealed a pseudopaline-dependent zinc uptake, with a 60% decrease of intracellular zinc content in the *ΔcntL* mutant strain in comparison with the WT strain (Figure 4B). The complemented strain accumulated zinc to a level comparable to the WT. In these chelating conditions the pseudopaline-dependent nickel import is abolished (Figure 4A), hence proving a direct link between pseudopaline and zinc uptake in metal scarce conditions with competing zinc chelators. These conditions may prevail at the host-pathogen interface where metal binding proteins such as calprotectin are produced by the host (29, 30), or in AMS where metals are complexed in a nutritional immunity framework (1, 21).

Model of pseudopaline synthesis and transport pathway in *P. aeruginosa*

We next investigated the putative roles of the two membrane proteins that are found in the *cnt* operon of *P. aeruginosa* by determining the pseudopaline level in the extracellular and intracellular fractions of WT and mutant strains (Figure 5A and 5B, respectively). With regard to PaCntO, we found a small decrease in the extracellular content of pseudopaline in the Δ*cntO* mutant strain in comparison with the WT strain. However, we also found that this Δ*cntO* mutant strain was partly impaired in nickel accumulation (Figure S5). Altogether, and because PaCntO belongs to the TBDT family of extracellular transporter, its most probable role is in the import of pseudopaline-metal complexes, although it is not excluded that other proteins of this family could participate in this process. Next, we noted a large decrease in the extracellular pseudopaline level in the Δ*cntI* mutant strain in comparison with the WT strain, with a concomitant increase in the intracellular space, consistent with a role of PaCntI in pseudopaline export. It is also interesting to note that a Δ*cntI* mutant strain is virtually unable to grow in AMS (21). The most probable scenario is that this mutant is deficient in metal content, including zinc, but pseudopaline accumulation in the cytoplasmic space actually worsens the situation by chelating an already poorly available metal. This assumption is supported by our finding that a double Δ*cntL*Δ*cntI* mutant supresses the detrimental growth defect of the single Δ*cntI* mutant strain, *ie* the absence of pseudopaline restores the normal growth of a mutant devoid of the pseudopaline exporter (Figure S6). A model recapitulating the pseudopaline pathway is shown in Figure 5.

It is interesting to note the differences and similarities between staphylopine and pseudopaline and between their respective biosynthetic pathways (Figure S7). On one hand, pseudopaline differs from staphylopine by the incorporation of a L-histidine instead of a D-histidine moiety in staphylopine, thus explaining the absence of amino acid racemase in *P. aeruginosa*. Another particularity of pseudopaline is the use of an αKG moiety instead of pyruvate as substrate for the second reaction mediated by PaCntM. Together this leads to two species-specific metallophores that might give a selective advantage in a competing environment. The fact that staphylopine and pseudopaline belong to Gram-positive and Gram-negative bacteria has important consequences on their respective transport mechanisms across the two types of bacterial envelopes. Although the transporters of staphylopine are well identified, the outer membrane exporter pseudopaline and inner membrane importer of the pseudopaline-metal complex remains to be discovered (Figure 5). Recycling of the metallophore could also take place in *P. aeruginosa*, as recently exemplified in the case for pyoverdine (31). An interesting

aspect of this work is the discovery of two different pathways for the export of these nicotianamine-like bacterial metallophores. Whereas *S. aureus* uses a protein belonging to the MFS family (SaCntE) for staphylopine export, *P. aeruginosa* uses a protein belonging to the DMT family of transporters, with PaCntI possessing two predicted EamA domains for pseudopaline export. In the view of their importance in the growth or virulence of these important human pathogens (19, 21), they could emerge as attractive targets for novel antibiotic development.

Acknowledgements

This work was supported by the ANR-14-CE09-0007-03 grant allocated to PA, RV, RL and EBD and the grant from “Vaincre la Mucoviscidose” (RFI20160501495) allocated to RV and PA. We thank B. Douzi for fruitful discussions, B. Ize for RNA preparation and C. Soscia for technical support as well as O. Uderso, I. Bringer and A. Brun for material and media preparations.

Author contributions: P.A. and R.V. designed research; S.L., N.G., L.O., C.B., G.G., C.H., A.L., S.W., P.R., S.B., G.B., E.B-D. and R.V. performed research; S.L., N.G., L.O., C.B., C.H., A.L., S.W., P.R., S.B., G.B., E.B-D., R.L., D. P., P.A and R.V. analysed data and P.A. and R.V. wrote the paper.

306 **References**

307 1. Hood MI, Skaar EP (2012) Nutritional immunity: transition metals at the pathogen–
308 host interface. *Nat Rev Microbiol* 10(8):525–537.
309 2. Weinberg ED (1975) Nutritional Immunity: Host's Attempt to Withhold Iron From
310 Microbial Invaders. *JAMA* 231(1):39–41.
311 3. Budzikiewicz AG (2010) Siderophores from bacteria and from fungi. *Iron Uptake and*
312 *Homeostasis in Microorganisms* (Cornelis, P. and Andrews, S. C.), pp 1–16. Caister
313 Academic Press.
314 4. Cornelissen CN, Hollander A (2011) TonB-Dependent Transporters Expressed by
315 Neisseria gonorrhoeae. *Front Microbiol* 2:117.
316 5. Cunrath O, Geoffroy VA, Schalk IJ (2016) Metallome of *Pseudomonas aeruginosa*: a
317 role for siderophores. *Environ Microbiol* 18(10):3258–3267.
318 6. Schalk IJ, Hannauer M, Braud A (2011) New roles for bacterial siderophores in metal
319 transport and tolerance. *Environ Microbiol* 13(11):2844–2854.
320 7. Minandri F, et al. (2016) Role of Iron Uptake Systems in *Pseudomonas aeruginosa*
321 Virulence and Airway Infection. *Infect Immun* 84(8):2324–2335.
322 8. Kim HJ, et al. (2004) Methanobactin, a copper-acquisition compound from methane-
323 oxidizing bacteria. *Science* 305(5690):1612–1615.
324 9. Dassama LMK, Kenney GE, Ro SY, Zielazinski EL, Rosenzweig AC (2016)
325 Methanobactin transport machinery. *Proc Natl Acad Sci U S A* 113(46):13027–13032.
326 10. Si M, et al. (2017) Manganese scavenging and oxidative stress response mediated by
327 type VI secretion system in *Burkholderia thailandensis*. *Proc Natl Acad Sci U S A*
328 114(11):E2233–E2242.
329 11. Cherrier MV, Cavazza C, Bochot C, Lemaire D, Fontecilla-Camps JC (2008)
330 Structural characterization of a putative endogenous metal chelator in the periplasmic nickel
331 transporter NikA. *Biochemistry (Mosc)* 47(38):9937–9943.
332 12. Lebrette H, et al. (2015) Novel insights into nickel import in *Staphylococcus aureus*:
333 the positive role of free histidine and structural characterization of a new thiazolidine-type
334 nickel chelator. *Metallomics*. doi:10.1039/C4MT00295D.
335 13. Shaik MM, Cendron L, Salamina M, Ruzzene M, Zanotti G (2014) *Helicobacter*
336 *pylori* periplasmic receptor CeuE (HP1561) modulates its nickel affinity via organic
337 metallophores. *Mol Microbiol* 91(4):724–735.
338 14. Bobrov AG, et al. (2014) The Yersinia pestis Siderophore, Yersiniabactin, and the
339 ZnuABC system both contribute to Zinc acquisition and the development of lethal septicemic

plague in mice. *Mol Microbiol*. doi:10.1111/mmi.12693.

15. Bobrov AG, et al. (2017) Zinc transporters YbtX and ZnuABC are required for the virulence of *Yersinia pestis* in bubonic and pneumonic plague in mice. *Met Integr Biometal Sci* 9(6):757–772.

16. Kallifidas D, et al. (2010) The zinc-responsive regulator Zur controls expression of the coelibactin gene cluster in *Streptomyces coelicolor*. *J Bacteriol* 192(2):608–611.

17. Ghssein G, et al. (2016) Biosynthesis of a broad-spectrum nicotianamine-like metallophore in *Staphylococcus aureus*. *Science* 352(6289):1105–1109.

18. Remy L, et al. (2013) The *Staphylococcus aureus* Opp1 ABC transporter imports nickel and cobalt in zinc-depleted conditions and contributes to virulence. *Mol Microbiol* 87(4):730–743.

19. Ding Y, Fu Y, Lee JC, Hooper DC (2012) *Staphylococcus aureus* NorD, a Putative Efflux Pump Coregulated with the Opp1 Oligopeptide Permease, Contributes Selectively to Fitness In Vivo. *J Bacteriol* 194(23):6586–6593.

20. Bielecki P, et al. (2011) In-vivo expression profiling of *Pseudomonas aeruginosa* infections reveals niche-specific and strain-independent transcriptional programs. *PloS One* 6(9):e24235.

21. Gi M, et al. (2015) A novel siderophore system is essential for the growth of *Pseudomonas aeruginosa* in airway mucus. *Sci Rep* 5:14644.

22. Pederick VG, et al. (2015) ZnuA and zinc homeostasis in Pseudomonas aeruginosa. *Sci Rep* 5:13139.

23. Solovyev, V, Salamov A (2011) Automatic Annotation of Microbial Genomes and Metagenomic Sequences. *Metagenomics and Its Applications in Agriculture, Biomedicine and Environmental Studies* (Li, R.W.), pp 61–78. Nova Science Publishers.

24. Pawlik M-C, et al. (2012) The zinc-responsive regulon of *Neisseria meningitidis* comprises 17 genes under control of a Zur element. *J Bacteriol* 194(23):6594–6603.

25. Patzer SI, Hantke K (2000) The zinc-responsive regulator Zur and its control of the znu gene cluster encoding the ZnuABC zinc uptake system in *Escherichia coli*. *J Biol Chem* 275(32):24321–24332.

26. Ellison ML, et al. (2013) The transcriptional regulator Np20 is the zinc uptake regulator in *Pseudomonas aeruginosa*. *PloS One* 8(9):e75389.

27. Thompson J, Donkersloot JA (1992) N-(carboxyalkyl)amino acids: occurrence, synthesis, and functions. *Annu Rev Biochem* 61:517–557.

28. Barber MF, Elde NC (2015) Buried treasure: evolutionary perspectives on microbial

374 iron piracy. *Trends Genet TIG* 31(11):627–636.
375 29. Nakashige TG, et al. (2016) The Hexahistidine Motif of Host-Defense Protein Human
376 Calprotectin Contributes to Zinc Withholding and Its Functional Versatility. *J Am Chem Soc*
377 138(37):12243–12251.
378 30. Subramanian Vignesh K, Deepe GS (2016) Immunological orchestration of zinc
379 homeostasis: The battle between host mechanisms and pathogen defenses. *Arch Biochem*
380 *Biophys* 611:66–78.
381 31. Ganne G, et al. (2017) Iron Release from the Siderophore Pyoverdine in *Pseudomonas*
382 *aeruginosa* Involves Three New Actors: FpvC, FpvG, and FpvH. *ACS Chem Biol*
383 12(4):1056–1065.
384 32. Braud A, Hannauer M, Mislin GLA, Schalk IJ (2009) The *Pseudomonas aeruginosa*
385 pyochelin-iron uptake pathway and its metal specificity. *J Bacteriol* 191(11):3517–3525.
386 33. Jeong J-Y, et al. (2012) One-step sequence- and ligation-independent cloning as a
387 rapid and versatile cloning method for functional genomics studies. *Appl Environ Microbiol*
388 78(15):5440–5443.
389 34. Viarre V, et al. (2009) HxcQ liposecretin is self-piloted to the outer membrane by its
390 N-terminal lipid anchor. *J Biol Chem* 284(49):33815–33823.
391 35. Kaniga K, Delor I, Cornelis GR (1991) A wide-host-range suicide vector for
392 improving reverse genetics in gram-negative bacteria: inactivation of the blaA gene of
393 *Yersinia enterocolitica*. *Gene* 109(1):137–141.
394 36. Liberati NT, et al. (2006) An ordered, nonredundant library of *Pseudomonas*
395 *aeruginosa* strain PA14 transposon insertion mutants. *Proc Natl Acad Sci U S A* 103(8):2833–
396 2838.
397 37. Hoang TT, Kutchma AJ, Becher A, Schweizer HP (2000) Integration-proficient
398 plasmids for *Pseudomonas aeruginosa*: site-specific integration and use for engineering of
399 reporter and expression strains. *Plasmid* 43(1):59–72.
400 38. Figurski DH, Helinski DR (1979) Replication of an origin-containing derivative of
401 plasmid RK2 dependent on a plasmid function provided in trans. *Proc Natl Acad Sci U S A*
402 76(4):1648–1652.
403
404
405

406

407 **Figures and figure legends**

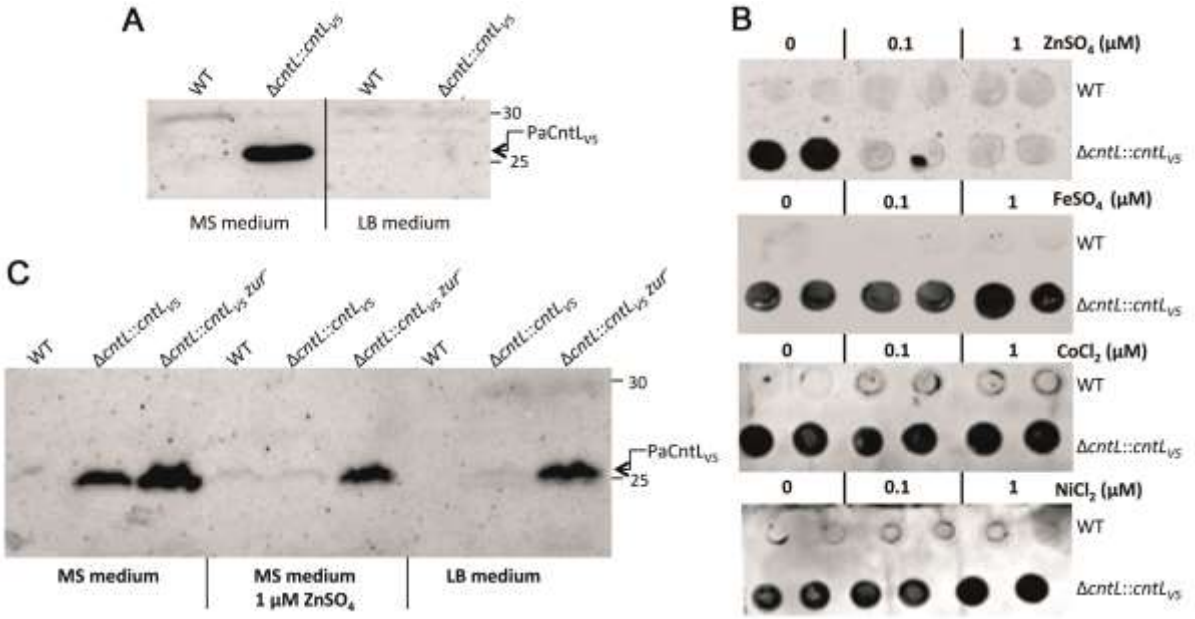

408

409 Figure 1: PaCntL production under various growth conditions. (A) Immunoblotting using
410 antibody directed against the V5 epitope for revealing PaCntL$_{V5}$ production under poor (MS)
411 and rich (LB) media. (B) Dot-blot revealing the Pa-CntL$_{V5}$ production in MS medium
412 supplemented by divalent metals. (C) Immunoblot detection of PaCntL$_{V5}$ production in PA14
413 WT and Zur deficient strains (*zur*$^-$) in various growth conditions.

414

415

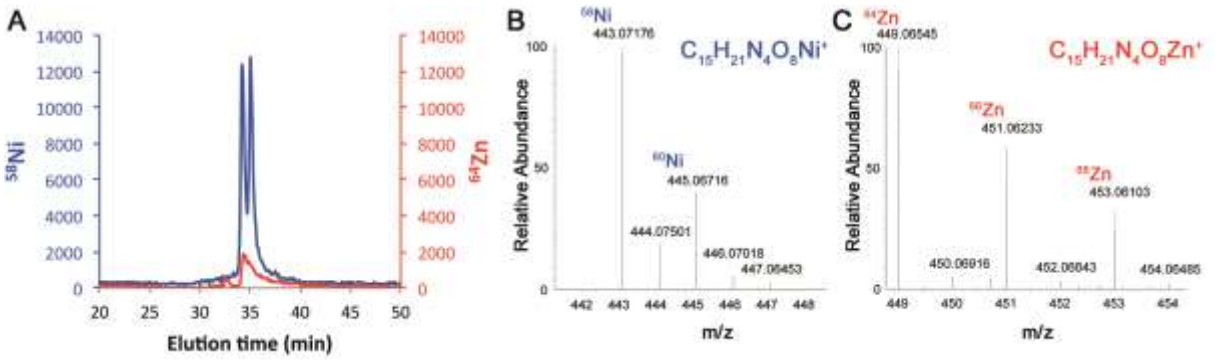

Figure 2: *In vivo* PaCntL-dependent detection of a nickel or zinc-bound metallophore in the extracellular fraction of *P. aeuginosa*. (A) HILIC/ICP-MS chromatogram of metal-bound metabolites. (B) HILIC-ESI/MS mass spectrum of a Ni-metallophore complex in the extracellular fraction of the WT strain but absent in the Δ*cntL* mutant. (C) HILIC-ESI/MS mass spectrum of a Zn-metallophore complex in the extracellular fraction of the WT strain but absent in the Δ*cntL* mutant. The empirical molecular formula of the CntL-dependant Ni- or Zn-metallophore complexes were deduced from the exact masse.

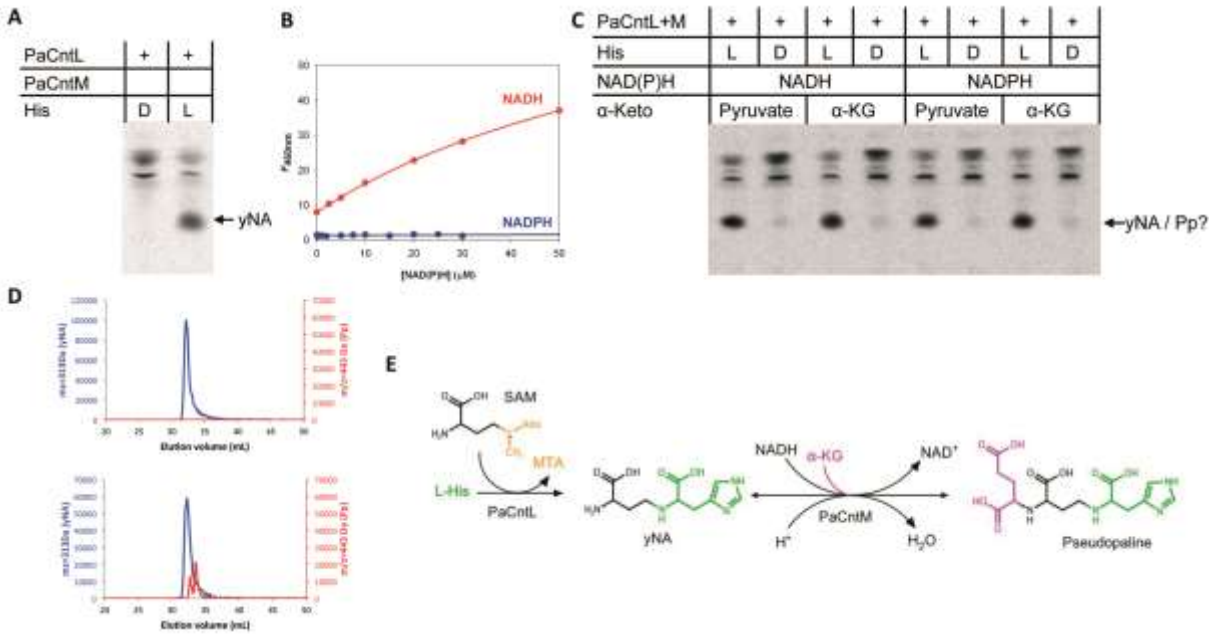

Figure 3: *In vitro* reconstitution of the pseudopaline biosynthesis pathway. (A) TLC experiment using PaCntL and [^{14}C]-SAM showing that PaCntL discriminates between D- and L-histidine substrate with the production of the reaction intermediate (noted yNA) only visible when using L-histidine. (B) Titration of NADPH (blue) and NADH (red) binding to PaCntM (5µM) followed by fluorescence resonance energy transfer. Fitting of the data obtained for NADH led to a K_d of 30µM. (C) TLC separation of reaction products incubating [^{14}C]-SAM using purified enzymes (PaCntL and PaCntM), different source of α-ketoacid (pyruvate or α-KG), cofactor (NADH or NADPH) and histidine (L-His or D-His). (D) HILIC/ESI-MS chromatograms of putative reaction products using PaCntL incubated with L-histidine, revealing the production of the yNA intermediate (top), and a mix of PaCntL and PaCntM incubated with all their putative substrate (SAM, L-histidine, NADH and α-Ketaoglutarate), revealing the specific detection of pseudopaline in this case (red trace, bottom). (E) Summary of the PaCntL/M-dependent biosynthesis pathway for the assembly of pseudopaline from L-his, SAM, NADH and α-KG.

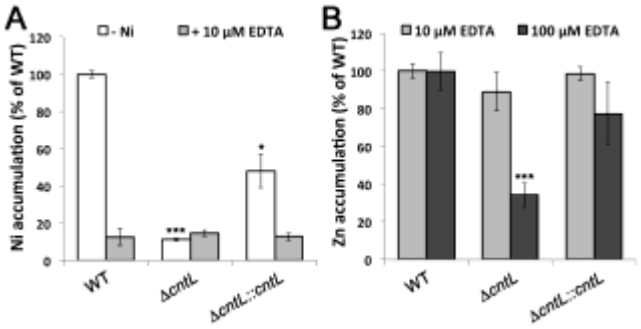

Figure 4: Pseudopaline is involved in nickel uptake in minimal media and in zinc uptake in chelating media. Intracellular nickel (A) or zinc (B) levels measured by ICP-MS in WT, *ΔcntL* and *ΔcntL::cntL* strains grown in MS medium supplemented or not with 10 or 100µM EDTA. Error bars, mean ± s.d. **P*<0.05, ***P*<0.01 and ****P*<0.001 as compared to the WT.

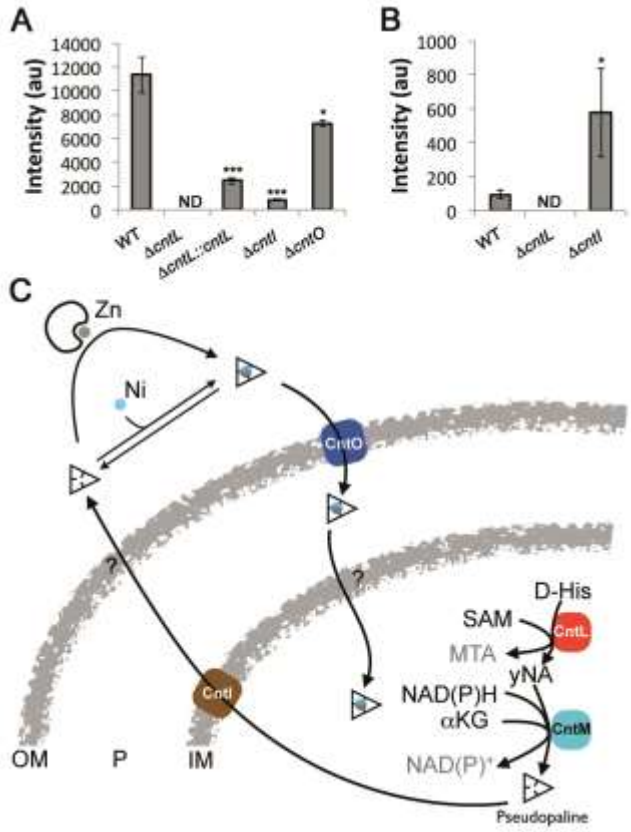

Figure 5: Model of pseudopaline synthesis, secretion and metal uptake in *P. aeruginosa.* (A) Extracellular detection of pseudopaline in the extracellular fraction of WT and mutant strains. Error bars, mean ± s.d. **P*<0.05, ***P*<0.01 and ****P*<0.001 as compared to the WT. (B) Intracellular detection of pseudopaline in the intracellular fraction of WT and mutant strains. ND: Not Detectable. (C) Model of pseudopaline production, secretion and recovery of nickel or zinc. Outer membrane (OM), inner membrane (IM), periplasm (P).

Materials and methods

Bacterial strains, plasmids and growth conditions

Bacterial strains, vectors and plasmids used in this study are listed in Table S2. *E. coli* strains were grown aerobically with shaking at 37°C in Luria-Broth (LB) with antibiotics as required (50 µg ml^{-1} ampicillin (Ap), 25 µg ml^{-1} kanamycin (Kan), 25 µg ml^{-1} tetracycline (Tc), 15 µg ml^{-1} gentamicin (Gm), 30 µg ml^{-1} streptomycin (Sm)). The *E. coli* strains CC118λ*pir* and SM10 were respectively used to propagate pKNG101 derivatives mutator plasmids and Mini-CTX1 plasmids. Recombinant plasmids were introduced in *P. aeruginosa* by triparental mating using pRK2013 and transconjugants selected on *Pseudomonas* isolation agar (PIA, Difco Laboratories) supplemented with antibiotics as required (500 µg ml^{-1} carbenicillin (Cb), 150 µg ml^{-1} Gm, 2000 µg ml^{-1} Sm, 200 µg ml^{-1} Tc). All the *P. aeruginosa* strains used in this study were derivatives of the parental PA14 strain. *P. aeruginosa* strains were grown aerobically with horizontal shaking at 37°C with antibiotics as required (150 µg ml^{-1} Cb, 50 µg ml^{-1} Gm, 500 µg ml^{-1} Sm, 50 µg ml^{-1} Tc). Growths were performed in TSB rich medium (Difco), minimal succinate (MS) medium (32) or chemically defined media (CDM) (18). When specified, Nickel on a $NiCl_2$ $6H_2O$ form, or Ethylenediaminetetraacetic acid (EDTA) were added to the media. Growth was monitored by OD600 measurement.

Plasmid construction

All plasmids constructed in this study were obtained by the one-step sequence- and ligation-independent cloning (SLIC) method described in ref (33). All PCR primers employed for plasmid construction are listed in Table S3. Genomic DNA was isolated and purified with Pure Link genomic DNA minikit (Invitrogen). PCR reactions for cloning were performed by using Q5® High-Fidelity DNA Polymerase (New England Biolabs, Inc (NEB)) and the products sequenced to verify the absence of any mutation (GATC-biotech).

Construction of cntL, cntI, cntO and cntI/L deletion mutant strains of P. aeruginosa

Two DNA fragments corresponding to upstream and downstream regions of *cntL, cntI* or *cntO* genes were amplified from PA14 chromosomal DNA with PCR primers SL1/2 & SL3/4 for *cntL*; SL12/13 & SL14/15 for *cntO* and SL19/20 & SL20/21 for *cntI* (Table S3). Upstream and downstream regions were ligated by overlapping PCR and cloned into linearized pKNG101 by the SLIC method. The resulting constructs were transformed into *E. coli* CC118λ*pir* and introduced into *P. aeruginosa* PA14 by conjugation. The strains in which the chromosomal integration event occurred were selected on *Pseudomonas* isolation agar Gm

plates. Excision of the plasmid, resulting in the deletion of the chromosomal target gene was performed after selection on Luria-Bertani (LB) plates containing 6% sucrose. Clones that became sucrose resistant and Sm sensitive were confirmed to be deleted for the gene of interest by PCR analysis. The Δ*cntI* Δ*cntL* double mutant strain was constructed by knocking-out *cntL* in the *cntI* mutant strain.

Construction of P. aeruginosa strains with cntL$_{V5}$ and cntL alleles inserted at aat site.

DNA fragments corresponding to the *cnt* promoter region (see sequence Figure S1) and *cntL$_{V5}$* or *cntL* alleles were generated by PCR from PA14 chromosomal DNA with PCR primers SL7/8 & SL9/10 or SL9/50 (Table S3). Upstream and downstream regions were ligated by overlapping PCR and cloned by the SLIC method in Mini-CTX1 vector. The resulting plasmid was introduced into *P. aeruginosa* PA14WT and PA14*zur*$^-$ strains by conjugation. The recombinant clones containing the mini-CTX1 inserted at the *attB* locus on the *P. aeruginosa* genome were selected on tetracycline-containing PIA. Excision of the unwanted plasmid DNA sequences (genes and associated promoter sequences that might interfere with expression of genes cloned into the MCS) located between the *FRT* sites (present on the mini-CTX1) was achieved by expressing Flp recombinase from a conjugative plasmid, pFLP2 which was introduced into *P. aeruginosa* PA14 by conjugation. The *P. aeruginosa* PA14 clones containing the pFLP2 were selected on carbenicillin-containing PIA. Finally, selection for pFLP2 deficient strains was done after selection on LB plates containing 6% sucrose. Colonies that became sucrose resistant and CB^S have lost the pFLP2 plasmid.

RNA isolation and RT-PCR reactions

Total RNA was prepared from *P. aeruginosa* strain PA14 mid-log phase cultures grown in MS medium using the SV Total RNA Isolation System (Promega). Contaminating DNA was removed by digestion with Dnase I (RTS Dnase kit - Ozyme). DNA-free total RNA was then used as a template for reverse transcriptase reactions using the Superscript III reverse transcriptase and random hexamers as described by the manufacturer (Invitrogen). Intragenic regions of *cntO, L, M* and *I* (see regions 1 to 4 Figure 1) were respectively amplified with primer couples SL42/43, SL44/45, SL46/47, SL48/49. Intergenic regions upstream *cntO,* between *cntO* and *cntL,* between *cntL* and *cntM,* between *cntM* and *cntI and downstream cntI* (see regions 5 to 9 figure 1) were respectively amplified with primer couples SL38/39, SL32/33, SL34b/35b, SL36/37, SL40/41.

Protein detection by immunoblotting

PA14Δ*cntL::cntL*$_{V5}$ was grown at 37°C in MS medium or Luria-Broth (LB) medium. When optical density at 600 nm (OD_{600}) reached 0.4 to 0.6 a volume of culture equivalent to 2 OD_{600} units was centrifuged for 2 min at 2.000 g. The pellet corresponding to whole cells was resuspended in 1X SDS-PAGE loading buffer containing β -mercaptoethanol and heated for 10 min at 95 °C. Proteins samples equivalent 0.1 OD_{600} units were separated by SDS-PAGE. Electrophoresis was performed using 12% SDS-polyacrylamide gel at room temperature and 25 mA/gel. Immunoblotting was performed as previously described (34), with rabbit primary and peroxidase-conjugated secondary antibodies respectively directed against V5 epitope (Bethyl/interchim) (dilution 1:5,000) and rabbit IgG (Sigma) (dilution 1:25000). The peroxidase reaction was developed by chemioluminescence (Pierce), scanned and analyzed with ImageQuant LAS 4000 camera and TL analysis software (GE Healthcare Life sciences).

Protein detection by dot blot

A nitrocellulose membrane was incubated 5 min with transfer buffer and dried at room temperature for 3 min. A 5 µL drop of SDS-PAGE protein sample (equivalent to 0.5 OD_{600} units was loaded onto nitrocellulose membranes. After drying, the proteins were transferred on the nitrocellulose for 5min at 80V and 0.1A using a Fast Blotter System (Pierce). Immunoblotting was perform with SNAP i.d.® 2.0 Protein Detection System. The membrane was blocked 5 min in TBS (1X) Tween 20 (0.1%) skim milk (0.5%), washed 4 times with TBS-Tween, incubated 10 min in TBS-Tween-milk with primary rabbit antibody directed against the V5 epitope (dilution 1:5,000), washed 4 times with TBS-Tween, incubated 10 min in TBS-Tween-milk with anti-rabbit peroxidase-conjugated antibody and the peroxidase reaction was developed by chemioluminescence, scanned with ImageQuant LAS 4000 camera and analyzed by the ImageQuant TL analysis software.

Viability essay on plate

Pre-culture of PA14 strains were performed overnight in MS medium under horizontal shaking at 37°C. The next day, a culture of fresh MS medium is inoculated by the pre-culture at OD_{600} of 0.1 and incubated for 6 hours under horizontal shaking at 37°C. Cultures were then adjusted to OD_{600} of 1 and subjected to 10% serial dilutions in fresh MS medium. 10 µl of culture samples were spotted on MS 5% agar plate an incubated overnight at 37°C.

Sample preparation for analysis by HILIC/ICP-MS, HILIC/ESI-MS and determination of metal concentrations by ICP-MS

All the *P. aeruginosa* strains derivatives of the parental PA14 strain were grown aerobically with horizontal shaking at 37°C in freshly made Minimal Succinate (MS) medium. All media used in this study were filtered at 0.22µm with polycarbonate units before used, and stored at 4°C away from light in polycarbonate bottles. Pre-culture of 20mL were inoculated from fresh MS-5% agar plates and grown until late exponential phase in polycarbonate erlenmeyers. Culture of 25mL were inoculated at OD=0.1 and grown for 8h in freshly made MS or CDM media supplemented or not with EDTA or nickel before inoculation. After 8h, OD_{600} were measured before cells were harvested by centrifugation (2,000*g*, 30min, 4°C). The supernatant was collected, filtered and stored at -80°C. The pellet was washed twice with 1.3mL MS media + 1mM EDTA followed by a wash with 1.3mL MS media. OD_{600} were measured, and cells ruptured by successive sonication cycles. The lysates were then centrifuged at 16,000g for 30min at 4°C and supernatants were collected and stored at -80°C. These cell lysate and supernatant fractions were used for analysis of metal complexes using HILIC/ICP-MS and HILIC/ESI-MS as described below. For metal quantitation, growth of WT and mutant strains was done as described above. After 9h of growth, OD_{600} was measured before cells were harvested by centrifugation (2,000*g*, 30min, 4°C). The pellet was washed 2 times with 1.3mL MS media + 1mM EDTA followed by a wash with 1.3mL MS media. After the OD_{600} was measured, cells were dried overnight at 95°C. The metal quantification was determined by inductively coupled plasma mass spectrometry as described elsewhere (17).

Analysis of metal complexes using HILIC/ICP-MS and HILIC/ESI-MS

Microbore HILIC separations were performed using an Agilent 1100 capillary HPLC system (Agilent, Tokyo, Japan) coupled either to ICP-MS detection (7500cs instrument, Agilent) or to an LTQ Orbitrap Velos mass spectrometer (Thermo Fisher Scientific, Bremen, Germany). The column used for HILIC separation was a TSK gel amide 80 (250 mm × 1 mm i.d., 5 µm) from Tosoh Biosciences (Stuttgart, Germany). Gradient elution, at a flow rate of 50 µl min^{-1}, was carried out using eluent A, acetonitrile, and eluent B, 5 mM ammonium formate (pH 5.5). Samples were diluted with acetonitrile and water to obtain a 1:2, sample to acetonitrile ratio, and centrifuged. A 7 µl aliquot of the supernatant was injected into the HILIC column each time. To get accurate masses during HILIC/ESI MS analysis, MS and MS/MS spectra were recalibrated offline using precursor/fragment ions with known formula. Putative metal species

were fragmented during a subsequent chromatographic run with collision induced dissociation (CID) mode at 35% energy. Signals were recorded at m/z corresponding to pseudopaline complexes with Ni and Zn ($C_{15}H_{20}N_4O_8Ni^+$ and $C_{15}H_{20}N_4O_8Zn^+$ respectively). Detailed procedures for chromatographic and MS analyses were described elsewhere (17).

Protein cloning, expression and purification

The *cntL* gene of *P. aeruginosa* P14 strain was amplified from genomic DNA and cloned in the vector pET22b$^+$ using the NdeI and XhoI restriction sites. This lead to a protein fused with a C-Terminal His_6 tag. The *cntM* gene of *P. aeruginosa* P14 strain was amplified from genomic DNA and cloned in the vector pET-TEV using the NdeI and XhoI restriction sites. This lead to a protein fused with a N-Terminal His_6 tag that could eventually be cleaved by TEV protease. Both vectors were transformed into *E. coli* BL21 strains for protein expression. The strain carrying the pET22b$^+$*cntL* plasmid were allowed to grow in LB medium containing 100 µg/ml ampicilline to an OD_{600} of 0.7 before inducing expression with 1mM Isopropyl-ß-D-thiogalactopyranoside (IPTG) followed by 20 hours incubation at 16°C. The strain carrying the pET-TEV*cntM* plasmid were allowed to grow in autoinducible medium containing 100 µg/ml ampicilline for overnight growth at 37°C. In both cases, the cells were pelleted, resuspended in buffer A (50 mM phosphate, 450 mM NaCl, 20 mM imidazole, pH 8.0), and disrupted with a French Press at 7 Mpa. The resulting soluble fraction was loaded on a Nickel charged column (HisTrap column, GE Healthcare) and the protein was eluted by an imidazole step gradient (50 mM wash and 200 mM elution). Gel filtration experiments were done using a Hiload 26/60 superdex200 column (GE Healthcare) using buffer B (50mM HEPES, 50mM NaCl, pH7.0)

Fluorimetry and TLC experiments

Fluorescence resonance energy transfer (FRET) experiments were performed using a Varian Cary Eclipse spectrofluorimeter with an excitation wavelength of 280 nm (tryptophan excitation, emission at 340 nm that is transferred to the NAD(P)H and recording of the emission at 460nm. Ligand binding was determined from the partial enhancement of this fluorescence emission. The amplitude of the FRET was fitted with a simple binding model using SigmaPlot software. TLC experiments were done as described elsewhere (17).